Title

In silico screening of the impact of hERG channel kinetic abnormalities on channel block and susceptibility to acquired long QT syndrome

Permalink

https://escholarship.org/uc/item/181881wc

Authors

Romero, Lucia
Trenor, Beatriz
Yang, Pei-Chi
et al.

Peer reviewed

In silico screening of the impact of hERG channel kinetic abnormalities on channel block and susceptibility to acquired long QT syndrome

Lucia Romero[a,*], **Beatriz Trenor**[a], **Pei-Chi Yang**[b], **Javier Saiz**[a], and **Colleen E. Clancy**[b]

Lucia Romero: lurope@eln.upv.es; Beatriz Trenor: btrenor@eln.upv.es; Pei-Chi Yang: pcyang@ucdavis.edu; Javier Saiz: jsaiz@gbio.i3bh.es; Colleen E. Clancy: ceclancy@ucdavis.edu

[a]Instituto de Investigación Interuniversitario en Bioingeniería y Tecnología Orientada al Ser Humano (I3BH), Universitat Politècnica de València, Camino de Vera s/n, 46022 Valencia, Spain

[b]Department of Pharmacology, University of California, Davis, Genome Building Rm 3503, Davis, CA 95616-8636, USA

Abstract

Accurate diagnosis of predisposition to long QT syndrome is crucial for reducing the risk of cardiac arrhythmias. In recent years, drug-induced provocative tests have proved useful to unmask some latent mutations linked to cardiac arrhythmias. In this study we expanded this concept by developing a prototype for a computational provocative screening test to reveal genetic predisposition to acquired long-QT syndrome (aLQTS). We developed a computational approach to reveal the pharmacological properties of I_{Kr} blocking drugs that are most likely to cause aLQTS in the setting of subtle alterations in I_{Kr} channel gating that would be expected to result from benign genetic variants. We used the model to predict the most potentially lethal combinations of kinetic anomalies and drug properties. In doing so, we also implicitly predicted ideal inverse therapeutic properties of K channel openers that would be expected to remedy a specific defect. We systematically performed "*in silico* mutagenesis" by altering discrete kinetic transition rates of the Fink et al. Markov model of human I_{Kr} channels, corresponding to activation, inactivation, deactivation and recovery from inactivation of I_{Kr} channels. We then screened and identified the properties of I_{Kr} blockers that caused acquired long QT and therefore unmasked mutant phenotypes for mild, moderate and severe variants. Mutant I_{Kr} channels were incorporated into the O'Hara et al. human ventricular action potential (AP) model and subjected to simulated application of a wide variety of I_{Kr}–drug interactions in order to identify the characteristics that selectively exacerbate the AP duration (APD) differences between wild-type and I_{Kr} mutated cells. Our results show that drugs with disparate affinities to conformation states of the I_{Kr} channel are key to amplify variants underlying susceptibility to acquired long QT syndrome, an effect that is especially pronounced at slow frequencies. Finally, we developed a mathematical formulation of the M54T MiRP1 latent mutation and simulated a provocative test. In this setting, application of

dofetilide dramatically amplified the predicted QT interval duration in the M54T hMiRP1 mutation compared to wild-type.

Keywords

Mutations; Drug-induced long-QT syndrome; Drug-induced arrhythmias; Computer modeling; Potassium channels; Genetics

1. Introduction

Drug-induced or acquired long-QT syndrome (aLQTS) is a disorder characterized by abnormally prolonged ventricular repolarization secondary to drug application that can lead to potentially lethal arrhythmias, such as torsade de pointes (TdP) [1]. This side-effect has resulted in black box warnings limiting the use of many drugs intended for treatment of cardiac dysrhythm, psychiatric disorders, gastrointestinal symptoms and infection [2] (http://www.qtdrugs.org). Drugs have even been removed from the market due to unintended effects on cardiac repolarization [3].

Because the rapidly activating component of the cardiac delayed rectifier current (I_{Kr}) arising from the gene hERG is a well-known promiscuous drug target, there has been deliberate focus on the off-target drug effects on hERG. Importantly, susceptibility to aLQTS has been linked to normally benign DNA variants in the genes encoding hERG and its ancillary subunits that modify risk to aLQTS and arrhythmias [1,4,5]. Indeed, approximately 15% of patients with aLQTS have been shown to exhibit allelic variants in coding regions of genes linked to congenital forms of long-QT syndrome (LQTS) [5].

Accurate identification of individuals who are susceptible to aLQTS is crucial for reducing the risk of cardiac arrhythmias [6]. Unfortunately, diagnosis based on baseline QT interval is not definitive [7] and genetic testing is difficult, expensive and is not always accessible [8]. In the last decade, drug-induced provocative tests have been proposed to unmask some types of latent mutation carriers. These provocative tests consist of the addition of a drug that uncovers an otherwise concealed disease. During the provocative test, the functional effects of a presumed defective ion channel are amplified, leading to measurable alterations in the electrocardiogram relative to changes observed with a normal channel. For example, catecholamines, such as epinephrine, can be used to reveal LQT1, which is due to I_{Ks} impairment [8], potent sodium blockers [9], such as flecainide, and also potent sodium blockers with calcium blockers [10] have been used to unmask Brugada syndrome, and sotalol [11] and erythromycycin [12], potent I_{Kr} blockers, have been shown to uncover altered repolarization.

Here, we employed a mathematical modeling approach to take existing tests a step further. We attempt to reveal the pharmacological properties of I_{Kr} blocking drugs that not only reveal predisposition to aLQTS, but also reveal the specific kinetic anomaly underlying the increased risk. In doing so, we also implicitly predict ideal therapeutic properties of K^+ channel openers that would be expected to remedy the defect. We systematically carried out "*in silico* mutagenesis" by altering discrete kinetic transition rates corresponding to

activation, inactivation, deactivation and recovery from inactivation of I_{Kr} channels. Our model predicts the most potentially lethal combinations of kinetic abnormalities and drug properties. Moreover, it identifies the specific properties of an I_{Kr} blocker that most exacerbate mutant phenotypes arising from specific defective I_{Kr} kinetics (activation, deactivation, inactivation and recovery from inactivation). Such a test can be used to unmask the mutant phenotype for latent, mild, and moderate mutants. Importantly, our method consists of a library of "off-the-shelf" mutant and drug interaction templates that can be readily expanded to predict drug interactions with any identified I_{Kr} mutation. To apply our approach in a true clinical setting, we carried out an *in silico* screen for the naturally occurring hERG mutation, the M54T MiRP1 mutation, which has been implicated in drug-induced LQTS and arrhythmia. We used the model to propose a provocative test to unmask the M54T mutation, which the model predicts will be most successful with a drug binding simultaneously to both the open and closed states with lower affinity to the open state (Actilide_Oc) or a drug binding simultaneously to both the open and inactivated states with lower affinity to the open state (Inactilide_Oi), like dofetilide. We also predict that use of a potassium channel opener as an adjunctive therapy can effectively blunt the effects of dofetilide-induced action potential prolongation of the M54T hMiRP1 mutation. Finally, the influence of heart rate and the concomitant effects of silent mutations in genes encoding other ionic currents were also investigated.

2. Methods

The human ventricular I_{Kr} was simulated using the five-state Markov chain proposed by Fink et al. [13]. Transition rate constants are provided in the supplemental material (Table S1). The Fink I_{Kr} Markov model was incorporated into the O'Hara et al. human ventricular action potential (AP) model [14] and its maximum conductance was scaled to elicit the same peak I_{Kr} value as the original O'Hara model at 1 Hz.

Activation ($\alpha\alpha$), deactivation ($\beta\beta$), inactivation (α_i) and recovery from inactivation (β_i) transition rates were modified to simulate genetic defects altering the activation, deactivation, inactivation and recovery from inactivation processes, respectively. In each case, transition rates were scaled to produce a 10 ms, 20 ms and 50 ms prolongation of action potential duration at 90% repolarization (APD_{90}) at 1 Hz, which gives rise to 12 prototypical I_{Kr} mutations. Scale factors are provided in the supplemental material (Table S2). Moreover, additional summative effects of I_{Ks} and I_{NaL} silent mutations were simulated by modifying the slow component of the delayed rectifier current (I_{Ks}) and the late sodium current (I_{NaL}). I_{Ks} and I_{NaL} were independently scaled to produce a 20 ms APD_{90} prolongation in WT cells. Then, all possible I_{Kr} mutants were simulated alone or in addition to these I_{Ks} and I_{NaL} modifications to simulate the combined effects of I_{Kr}, I_{Ks} and I_{NaL} silent mutations. A total number of 38 prototypical mutants, namely, 12 I_{Kr} mutations, 12 I_{Kr} mutations combined with I_{Ks} reduction, 12 I_{Kr} mutations combined with I_{NaL} increase, one I_{Ks} mutation alone and one I_{NaL} mutation alone, were simulated.

The M54T hMiRP1 mutation was modeled using a modified Nelder–Mead simplex method to modify the Markov model transition rates in the Fink I_{Kr} model by minimizing the sum of the least-square errors between the experimental [4] and the simulated steady state activation

curves, steady state inactivation curves and deactivation time constants. Then, to validate the M54T hMiRP1 mutation computational model, the simulated reduction of current density at —40 mV was compared to additional experimental results [1]. As experiments were performed at 22 °C [4] and room temperature [1], temperature was exclusively fixed to 22 °C to compare the simulated kinetics of the mutation to experiments. Physiological action potential simulations were subsequently performed at 37 °C. Rate transitions for WT and the mutated cells are available in the supplemental material (Table S1).

In order to simulate known drug interactions with I_{Kr}, we used measured affinities and drug diffusion rates used to constrain the drug "on" and "off rates. Diffusion rates (D) indicate drug on rates "k" = [drug] * D and affinities (K_d) to discrete conformations that determine drug off rates "r" = K_d * D. Association (k) and dissociation (r) rate values for each I_{Kr}–drug interaction as tested in the model are in the supplement (Table S3). On and off rates were varied in simulations of "theoretical" drugs. A total number of 21 drug interactions with I_{Kr} were simulated; dofetilide and 20 "theoretical drugs". In addition, two potassium channel openers, RPR260243 and a virtually designed "activator" drug were simulated in some cases. In order to simulate the effects of RPR260243 we used the same binding and unbinding rate constants as Perry et al. [15] and activator bound channels were reconstructed applying the same modifications as Perry and coworkers to the WT channels, namely slowed deactivation, slowed activation and reduced inactivation [15]. The model of the virtual activator resulted from eliminating the reduced inactivation from the RPR260243 model and was called RPR260243_mod.

1596 provocative tests were carried out with the application of low and high concentrations of each simulated drug to WT cells and to every mutant at 1 Hz. For reproducibility, the low and high doses of a certain drug was defined as the drug concentration that produced the same steady state WT APD_{90} prolongation as 16 nM (in line with its therapeutic dose [3]) and 48 nM dofetilide, respectively. Low dose values for each simulated drug are available in the supplemental material (Table S3). 442 additional provocative tests were performed at 2 Hz and 0.67 Hz by applying low doses of those drugs that most amplified the effects of I_{Kr} mutants on ADP_{90} at 1 Hz to investigate the rate dependence of aLQTS in genetically predisposed cells. Furthermore, as APD adaptation to abrupt changes in pacing rate has been proposed as a clinical marker for arrhythmic risk [16], APD rate adaptation was also characterized by recording APD_{90} during the transition from the steady-state at 1 Hz to 1.7 Hz and from 1.7 Hz to 1 Hz after 10 min of pacing at 1.7 Hz. This protocol is similar to that used in clinical and experimental studies [17,18] and in other theoretical works [19,20]. APD_{90} dynamics were characterized by the fast and slow time constants of the APD_{90} adaptation to the accelerating and decelerating rate transitions ($\tau_{fast\_accelerating}$, $\tau_{slow\_accelerating}$, $\tau_{fast\_decelerating}$ and $\tau_{slow\_decelerating}$, respectively) [19,20]. When the duration of APD adaptation was longer than 10 min, independent prolongation of each transition was conducted to obtain the slow time constants.

Action potential simulations were carried out in isolated endocardial cells at 1 Hz and pseudo-ECGs were computed using a 1-dimensional model of the transmural wedge preparation, as described in [14].

3. Results

We updated our previous dofetilide model [21] to additionally include the experimentally observed 70-fold preferential binding to the inactivated state relative to the open state [22] and to mimic the clinically observed 16% prolongation of the QT interval produced by the therapeutic dose 8.22 nM [23] (summarized in Fig. 1D). Figs. 1 A–C show the kinetics of the simulated (lines) I_{Kr} block by 50 nM dofetilide (A and B) and the washout of 3 μM (C) (solid lines) together with experimental results (symbols) for comparison: [24](A), [25] (B) and [26] (C). Protocols are described in [24–26]. Figs. 1B and C show that our model also reproduces the experimentally observed voltage dependency of the onset of block by dofetilide [25] and the extremely slow and incomplete dissociation of dofetilide reported by many experimental works [24,26,27], respectively. To validate our simulations of drug interactions with I_{Kr}, the sensitivities of two hERG mutations, N588E and N588K, to I_{Kr} dofetilide block were also simulated. The N588E model was obtained by modifying the rates between the open and inactivated state to produce a —36 mV shift of the conductance voltage curve (top panel of Fig. 1E) and the N588K mutation model was obtained by applying to the human ventricular I_{Kr} model the same alterations as in [22]. Protocols are described in [22]. Bottom table of Fig. 1D summarizes the modifications introduced in the I_{Kr} model to simulate the effects of the N588E and N588K mutations. The mutated residue is remote from the drug-binding pocket in the channel pore [22], and experiments suggest that values of drug affinities for the mutated I_{Kr} channels are unchanged from WT [22]. We also made this assumption in the model. The top and bottom panels of Fig. 1F include experimental data and simulation of the Hill plots of dofetilide binding for WT, N588E and N588K, respectively. The differential blocks in N588E and N588K mutated I_{Kr} produced by dofetilide predicted by our model simulations are in close agreement with the experiments performed in Chinese hamster ovary (CHO) cells [22].

As shown in Fig. 2A, the Markov model representation of I_{Kr} from Fink et al. includes three closed states (C_3, C_2 and C_1), a conducting open state (O) and an inactivation state (I). This channel model was incorporated into the O'Hara et al. human ventricular action potential (AP) model [14] (black traces in the top row of Fig. 3) and its maximum conductance was scaled to elicit the same peak I_{Kr} value as the original O'Hara model at 1 Hz (black traces in the middle row of Fig. 3).

We carried out "*in silico* mutagenesis" by modifying discrete transition rates (orange arrows in Fig. 3 model schematic) in the computational model that led to targeted modification of channel activation, inactivation, deactivation or recovery from inactivation (from left to right) as indicated and resulting prolongation of the APD_{90} by 50 ms, 20 ms and 10 ms These changes were intended as prototypical latent, mild and moderate (red) allelic variants in hERG that may underlie a predisposition to aLQTS. The effects of moderate variants led to a 50 ms APD_{90} prolongation (top row), I_{Kr} reduction (middle row) and open state probability (bottom row). Deactivation mutants (second column) result in the smallest I_{Kr} among the simulated functional mutants and with the most altered morphology (red arrow in middle row). Deactivation mutants are most severe because I_{Kr} current arises at the critical late juncture in the action potential to cause final AP repolarization precisely because of the imbalance between rapid recovery from channel inactivation and subsequent slow

deactivation. This imbalance normally results in channels residing in the open state during repolarization. Mutations that increase the rate of deactivation are dire: they lead to a marked reduction in channel open probability (red arrow in bottom row) by promoting channel closure.

Figs. 2B–F shows the I_{Kr} Markov model described above with multiple distinct drug bound configurations (lower row of states in each panel indicated by subscript "d") in panels B though F. Because ion channel targeting drugs display complex properties determined by preferential binding to distinct conformation states and/or distinct affinity to discrete states, we simulated a wide variety of likely combinations of drug-channel interactions (Figs. 2B–F): drugs that exclusively bound in the closed (Fig. 2B), open (Fig. 2C) or inactivated (Fig. 2D) states, as well as drugs binding simultaneously to both the closed and open states (Fig. 2E), or to both the open and inactivated states (Fig. 2F), were analyzed in detail by testing a range of association and dissociation rates for the various drug configurations. The initial estimated association and dissociation rates were assumed to be similar to the association rate of dofetilide and an intermediate value of the dissociation rates of dofetilide. The values 0.511 μM^{-1} s^{-1} and 0.003606 s^{-1} were used as the baseline association and dissociation rates. Rates were then varied in the test simulations by increasing them 10-, 50-, or 100-fold or reducing rates 10- or 100-fold.

3.1. Latent defective activation

In the first column of Fig. 4, the effects of latent (blue), mild (green) and moderate (red) variants of activation (orange arrow in Markov diagram indicates the altered transition rate) led to varying degrees of APD_{90} prolongation (10, 20 and 50 ms, respectively), consistent with the degree of change to the activation rate (first row). We next carried out multiple simulations with 21 I_{Kr} blocking drugs spanning a variety of inherent kinetic properties, conformational state specificities and concentrations. The model predicts that most drugs were unable to differentiate between normal and mutant channels. Low doses of drugs that exclusively bound to a single I_{Kr} state, drugs that simultaneously bound to open and inactivated channels, and drugs that bound with low affinity to the closed state but with high affinity to the open state produced similar APD_{90} prolongation in normal and mutant channels.

However, the model predicted that drugs binding to closed and open states with lower affinity to the open state (Actilide_Oc) amplified mutant effects on APD_{90} prolongation in activation mutants compared to WT (the pink arrow in the Markov scheme indicate a lower affinity of the drug in that state). A drug (depicted in the Markovian scheme at the top of the first column) with these properties was identified in the simulations to best unmask the mutant phenotype. Exposure to 3 nM (low dose) Actilide_Oc_1 (supplemental material, Table S3) (Fig. 4, middle row of the first column) increased the APD_{90} difference between WT and impaired activation cells from 10 ms to 16 ms, from 20 ms to 33 ms and from 50 ms to 83 ms. Differences in APD_{90} between WT and impaired activation cells were also sensitive to Actilide_Oc_1 concentration. Indeed, addition of 12 nM (high dose) Actilide_Oc_1 (Fig. 4, bottom row of the first column) increased the APD_{90} differences between WT and cells with defective activation from 10 ms to 20 ms, from 20 ms to 43 ms

and from 50 to 118 ms, respectively. Addition of other drugs binding in the closed and open state with lower affinity to the open state (Actilide_Oc_2, Actilide_Oc_3 and Actilide_Oc_4) but with different dissociation rates (supplemental material, Table S3) produced similar APD$_{90}$ differences between WT and cells with defective activation as Actilide_Oc_1 in the steady state. However, the duration of the transitory period from drug application to the steady state depended on the specific association and dissociation rate values of the drug and faster rates led to shorter transitory periods.

3.2. Latent defective deactivation

In the second column of Fig. 4, the effects of latent, mild and moderate variants of deactivation (orange arrows in the Markov diagram indicate the altered transition rate) led to corresponding varying degrees of APD$_{90}$ prolongation (first row of the second column). We next simulated the effect of a wide variety of I$_{Kr}$ blocking drugs on these deactivation mutants. Surprisingly, the model predicts that most drugs preferentially prolonged the steady state APD$_{90}$ in mutated cells with marked faster deactivation. This result indicates that allelic variants affecting deactivation would lead to increased sensitivity to a wider range of I$_{Kr}$ blockers, and consequently, an increased likelihood of aLQTS. This is in accordance with the fact that deactivation mutants (Fig. 3, second column) result in the smallest I$_{Kr}$ among the simulated functional mutants and with the most altered morphology (Fig. 3, red arrow in middle row).

Drugs binding in the closed and open states with significantly lower affinity in the open state produced the largest APD$_{90}$ differences between WT and mutated cells with faster deactivation, as in the case of activation mutants, but substantially longer APD$_{90}$ prolongations were observed in deactivation mutants. The second column of Fig. 4 shows the simulation results of exposure of deactivation mutations to one drug of this type, Actilide_Oc_1. In this case, application of 3 nM (low dose) Actilide_Oc_1 (Fig. 4, middle row of the second column) amplified the APD$_{90}$ difference between WT and deactivation mutant cells from 10 ms to 113 ms (blue), from 20 ms to 181 ms (green) and from 50 to 294 ms (red). Addition of 12 nM (high dose) of this drug (Fig. 4, bottom row of the second column) enhanced the APD$_{90}$ difference between WT and deactivation mutant cells from 10 ms to 177 ms (blue) and generated patterns of early-afterdepolarizations (EADs) in deactivation mutants whose APD$_{90}$ is 20 ms and 50 ms longer than WT under drug-free conditions (green and red, respectively).

Differential APD$_{90}$ prolongation was also induced by drugs binding in the open and inactivated state with a much lower affinity in the open state. Indeed, the addition of 3.6 nM (low dose) Inactilide_Oi_1 increased the APD$_{90}$ differences between WT and cells with defective deactivation from 10 ms to 102 ms, from 20 ms to 167 ms and from 50 to 262 ms (not shown). Exposure to 10.55 nM (high dose) of this drug also further increased the APD$_{90}$ differences between WT and deactivation mutants from 10 ms to 164 ms and generated EADs in AP in deactivation mutants whose APD$_{90}$ is 20 ms and 50 ms longer than WT under drug-free conditions (not shown). Drugs exclusively binding in one I$_{Kr}$ state still unmasked this type of defect in moderate mutants, but they produced smaller APD prolongations in deactivation mutants than the previous drugs. For example, Drug_C1

(supplemental material, Table S3) produced a 96 ms APD_{90} difference between WT and the deactivation mutation cell that is 50 ms longer than WT in drug-free conditions. Finally, drugs binding in the closed and open state with a much lower affinity in the closed state and drugs binding in the open and inactivated state with a much lower affinity in the inactivated state did not help to discern between WT and mutants, as 67 ms and 64 ms steady state APD_{90} differences between WT and the 50 ms APD_{90} prolongation mutation under drug-free conditions were observed during low dose drug exposure, respectively. Again, drug-induced steady-state APD prolongation depended on the states where the drug bound and the preferential binding to a channel state, regardless of the diffusion rate of the drug.

The previously explained amplification of the effects of defective I_{Kr} deactivation on APD_{90} prolongation produced by most drugs is directly related to the extent of the reduction in current. Indeed, Actilide_Oc, which is the type of drug that most amplifies defective I_{Kr} deactivation indicated by APD_{90} prolongation, is the one that most reduces the fast deactivated I_{Kr} current, closely followed by Inactilide_Oi (see supplemental material, Fig. S2).

3.3. Latent defective inactivation

The first row of the third column of Fig. 4 shows the time course of the APs elicited by WT and cells harboring three modeled inactivation mutations yielding 10 ms, 20 ms and 50 ms APD_{90} prolongation relative to WT (orange arrows in Markov diagram indicate the altered transition rate). Our simulations predicted that low doses of simulated drugs that bound exclusively to one discrete I_{Kr} state and drugs binding both the closed and open state with low affinity to the open state were not able to amplify differences between WT and inactivation mutants and were thus unable to unmask the mutations. Indeed, exposure to 10 nM (low dose) of Drug_C1 (supplemental material, Table S3) only increased in 3 ms the APD_{90} difference between WT and the inactivation mutant whose APD_{90} was 50 ms longer than WT in drug-free conditions and Actilide_Oc_1 (supplemental material, Table S3) did not amplify it.

Drugs interacting with low affinity to closed and high affinity to the open states performed somewhat better, as 750 nM (low dose) of Actilide_Co (supplemental material, Table S3) only increased in 7 ms the APD_{90} difference between WT and the inactivation mutant whose APD_{90} was 50 ms longer than WT in drug-free conditions.

However, a drug with low affinity open state block (pink arrow in model schematic) and higher affinity inactivated state (black arrow) very effectively unmasked I_{Kr} mutants causing impaired inactivation. Specifically, application of 3.6 nM (low dose) and 10.55 nM (high dose) Inactilide_Oi_1 (supplemental material, Table S3) (Fig. 4, middle and bottom row of the third column, respectively) enhanced the APD_{90} differences between WT and defective inactivation cells from 10 ms to 15 ms and 19 ms (blue), from 20 ms to 28 ms and 39 ms (green) and from 50 to 76 ms and 113 ms (red), respectively. In this case, the steady state APD prolongation observed during drug exposure also depended most on the states where the drug bound and the preferential binding state regardless of its diffusion rate.

3.4. Latent defective recovery from inactivation

Low doses of each drug were applied to WT and cells containing a simulated mutagenesis affecting the rate constant controlling I_{Kr} recovery from inactivation (RFI, rate from I to O) indicated by the orange arrow in the schematic. Simulated mutations yielded 10 ms, 20 ms and 50 ms APD_{90} prolongation compared to WT (Fig. 4, first row of the fourth column). As expected, this simulated defect primarily affected the fractions of channels in the inactivated and open state, much like mutations that affected the inactivation transition. A drug with low affinity block in the open state (pink arrow) and preferential higher affinity block in the inactivated state (black arrow) as depicted in the Markovian scheme at the top of the fourth column of Fig. 4, amplified the mutation effect, observed by more APD_{90} prolongation in mutated cells with impaired recovery from inactivation than in WT cells. In this case, application of 3.6 nM (low dose) and 10.55 nM (high dose) Inactilide_Oi_1 (Fig. 4, middle and bottom rows of the fourth column, respectively) augmented the APD_{90} difference between WT and RFI mutant cells from 10 ms to 15 ms and 18 ms (blue), from 20 ms to 27 ms and 37 ms (green) and from 50 to 76 ms and 99 ms (red), respectively.

3.5. M54T hMiRP1 mutation

We also applied this procedure to the naturally occurring hERG mutation, the M54T MiRP1 mutation, which has been implicated in drug-induced LQTS and arrhythmia [1,4]. Fig. 5 compares the experimental (top row) and the simulated (bottom row) steady state activation curve (left column) and the deactivation time constant curve (right column) for WT (squares) and M54T hMiRP1 mutated channels (triangles). Protocols are described in Abbott et al. [4]. This mutation is known to moderately increase the voltage dependence of activation by reducing the activation slope without altering the half activation potential [4]. The experimentally measured activation slope was 9.5 mV and 7.5 mV for WT and M54T hMiRP1 mutated channels, respectively [4]. Therefore, the activation slope of these mutated channels is 75.8% the slope of the WT channels. The activation slope of the simulated M54T hMiRP1 mutated channels is 75.5% the slope of the simulated WT channels. Importantly, M54T hMiRP1 mutated channels are also known to deactivate approximately twice as fast as WT [4]. Our simulated M54T hMiRP1 mutated channels reproduce this alteration (right panels). In addition, experimental results evidence that M54T hMiRP1 mutated channels were like wild type in their steady state inactivation [4]. The simulated M54T hMiRP1 mutation did not alter the steady state inactivation curve in our model (not shown). Moreover, additional experiments reported a reduction of 39% in current density at —40 mV in M54T hMiRP1 mutated channels [1]. The alteration of the transition rates in our simulated M54T hMiRP1 mutated channels caused a similar reduction in current density (not shown), therefore the maximum conductance of the mutated channels was not modified. Rate constants for the simulated M54T hMiRP1 channels are provided in the supplemental material (Table S2). Quantitative differences between the experimental results of the M54T MiRP1 latent mutation and the simulations (Fig. 5) derive from the differences in the cells and subunits of the channels used in the characterization of the mutation and the data used to model the I_{Kr} used in our study. Indeed, the experimental data (shown in the top row of Fig. 5) was obtained from hMiRP1/hERG channels expressed in *Xenopus laevis* oocytes [4] and the I_{Kr} model proposed by Fink et al. [13] and used in our simulations for WT cells was

fitted to experimental data from hERG in HEK cells and human myocytes and incorporated relative changes resulting from the mutation into the baseline Fink model.

We incorporated the M54T hMiRP1 channels into the AP model. The M54T hMiRP1 mutated (orange) APD_{90} was 11.6 ms longer than WT (black) APD_{90} in isolated endocardial cells (Fig. 6A). As we did with the virtual mutations, we also observed the amplification of the APD_{90} differences between M54T hMiRP1 mutated and WT cells under drug exposure. The virtual drug types that most amplified the APD_{90} of M54T hMiRP1 mutants were Actilide_Oc and Inactilide_Oi. Specifically, low doses of both Actilide_Oc_2 and Inactilide_Oi_2 led to a 46 ms difference between M54T hMiRP1 mutants and WT cells. Addition of other types of drugs did not help to differentiate between M54T hMiRP1 mutants and WT cells. For example, exposure to low dose of Drug_C_2 only produced 3 ms additional difference in APD_{90} between M54T and WT cells compared to drug-free conditions. These results resembled those obtained with the prototypical latent fast deactivation mutant. It supports the validity of our method to predict the drug types that affect a particular mutation, as fast deactivation is the main I_{Kr} alteration produced by M54T hMiRP1 mutation [4]. We also simulated the effects of the real drug dofetilide in the presence of this naturally occurring mutation. Exposure to 16 nM (low dose) and 48 nM (high dose) dofetilide increased the APD_{90} difference between WT (black) and mutants (orange) from 11.5 ms (Fig. 6B) to 46 ms (Fig. 6C) and 65 ms (Fig. 6D), respectively. It is notable that dofetilide and Inactilide_Oi_2 produced similar results. Dofetilide could be classified as an Inactilide_Oi drug because it binds in the open and in the inactivated states [25] with a 70-fold preferential binding to the inactivated state relative to the open state [22].

As the ECG is the electrical signal used for clinical diagnosis rather than the APD in isolated cells, we also simulated the pseudo-ECG using a 1-dimensional model of the transmural wedge to investigate the potential use of this dofetilide modification to unmask silent mutation carriers. Our results (Fig. 6, bottom row) show that the M54T hMiRP1 mutation produced a 6 ms prolongation of the simulated QT interval duration (WT QT interval duration = 392 ms, Fig. 6D) under drug-free conditions. The presence of 16 nM (low dose) and 48 nM (high dose) of dofetilide amplified the QT interval duration difference between WT and mutant to 47 ms (Fig. 6E) and 105 ms (Fig. 6F), respectively. The generation of EADs in midmyocardial cells (see inset of Fig. 6F) in the transmural strand after the application of high dose modified dofetilide led to more aggravated differences in the QT interval between WT and M54T mutated cells than in the APD_{90} registered in isolated cells. The development of the EAD in the M cell only leads to an apparent increase in dispersion of repolarization, observed on the simulated ECG as a broadening of the t-wave (due to very long repolarization in the M-cell) and also an increase in the amplitude of the t-wave (resulting from the large voltage dispersion (gradient)) that occurs when the epicardial cell has repolarized and the M-cell is depolarized due to the EAD.

Simulated pseudo-ECGs at 1 Hz for WT in the presence of high doses of every drug considered in this study are shown in Fig. S5 in the supplemental material. Although they are very similar, small differences in the T-wave are observed. Indeed, the drugs that most increase the amplitude of the T-wave are Inactilide_Oi, Inactilide_Io and Actilide_Co, followed by drugs binding and unbinding in one state of the channel (Drug_C, Drug_O and

Drug_I). Actilide_Oc caused minimal increase in the amplitude of the T-wave (see Fig. S6 in the supplemental material).

We also simulated the addition of potassium channel activators to mitigate the effects of dofetilide exposure on M54T hMiRP mutated channels to dramatically prolong APD_{90}. As M54T hMiRP mutated channels exhibit fast deactivation, our analysis suggests that a channel opener that slows deactivation would be postulated as the ideal channel opener. Therefore, type 1 agonists, which slow deactivation and attenuate inactivation, would be more appropriate in this case than type 2 agonists, which attenuate inactivation without slowing deactivation [28]. Fig. 7A shows that addition of 230 nM RPR260243 (orange thick line), a type 1 agonist, following application of 16 nM dofetilide in M54T hMiRP1 mutated cells at 1 Hz (orange thin line) shortened APD_{90} to the level observed in WT cells in the presence of 16 nM dofetilide at 1 Hz (black thin line). In other words, adjunctive therapy with a type 1 hERG channel activator canceled the effects of the M54T mutation. This was also observed at 0.67 Hz and 2 Hz (2.3 ms and 7.8 ms APD_{90} difference, respectively). Importantly, the reduction in APD_{90} predicted by the model simulations in both WT and M54T hMiRP mutated cells in the presence of 230 nM RPR260243 was comparable (∼26 ms, see Fig. 7B at 1 Hz) and the shortening was dose-dependent (see Figs. 7B and C at 1 Hz). This prediction suggests that the type 1 hERG channel activator *did not discriminate between WT and mutant channels*, suggesting that the drug would not cause unexpected effects through interaction with the mutation.

Next, we used our *in silico* method to predict properties to improve the performance of this activator. Our simulations suggest that elimination of the effects of RPR260243 on inactivation (RPR260243_mod) would minimize the shortening of the APD_{90} in the absence of I_{Kr} blockers while reducing the APD_{90} prolongation of M54T hMiRP1 mutated cells and the related *in silico* mutant in the presence of dofetilide. Indeed, addition of 1.2 mM RPR260243_mod to 16 nM dofetilide in M54T hMiRP1 mutated cells normalized APD_{90} to WT in the presence of 16 nM dofetilide at 1 Hz (Fig. 7D), 0.67 Hz and 2 Hz (0.7 ms, 1.5 ms and 18.4 ms APD_{90} difference, respectively). *Importantly, this concentration of RPR260243_mod did not reduce the APD_{90} of WT and M54T hMiRP1 mutated cells in the absence of dofetilide* (Fig. 7E), except for a small 4 ms reduction at 2 Hz. In addition, a tenfold increase in RPR260243_mod concentration did not reduce the APD_{90} of WT cells in the absence of dofetilide at 1 Hz (Fig. 7F) and only reduced it in 6 ms at 2 Hz. Similar results were obtained when these channel openers were added to *in silico* mutated cells with hastened deactivation.

3.6. Effects of heart rate and combination of mutations

To further investigate the genetic predisposition to aLQTS, the influence of heart rate and the presence of silent mutations on other ionic currents were also analyzed.

3.6.1. Heart rate—We next tested the rate dependence of pharmacological amplification of I_{Kr} allelic variants on APD_{90} during exposure to the drugs that most amplified them at 1 Hz (Actilide_Oc, Inactilide_Oi and drugs exclusively binding and unbinding in the closed, open or inactivated states). Drugs were tested at fast (2 Hz) and slow frequencies (0.67 Hz).

Fig. 8 shows the rate dependence of the effects of activation (A), deactivation (B), inactivation (C) and recovery from inactivation (D) I_{kr} mutants producing a 50 ms prolongation of APD_{90} under drug-free conditions at 1 Hz on AP_{90} under drug-free conditions (black) and under exposure to low dose Actilide_Oc_1 (red), Inactilide_Oi_1 (green), and Drug_C1 (blue). Our simulations show that the same drugs that amplified mutant effects on APD_{90} prolongation at 1 Hz also amplified them at fast and slow frequencies, although the magnitude of the APD_{90} prolongation depended on the type of the drug, the mutant and the heart rate. In general, the slower the frequency, the larger the mutant amplification on APD_{90} predicted. As observed at 1 Hz, APD_{90} of deactivation mutants were preferentially prolonged by most drugs, especially by Actilide_Oc and Inactilide_Oi. Low doses of these drugs produced EADs at 0.67 Hz and APD_{90} longer than 500 ms at 2 Hz (Fig. 8B). Drugs binding in only one state also enhanced the APD differences between deactivation mutants and WT, although to a lesser extent (Fig. 8B). In addition, the effects of impaired activation on APD_{90} were especially amplified under exposure to Actilide_Oc, regardless of the pacing rate (Fig. 8A). Finally, Inactilide_Io was the type of drug that most amplified inactivation and recovery from inactivation mutant effects on APD_{90} prolongation at all frequencies (Figs. 8C and D).

Differences between WT cells and I_{Kr} mutants on APD heart rate adaptation to abrupt changes in pacing frequency under drug-free conditions and under exposure to selected I_{Kr}–drug interactions were also investigated (see supplemental material, Fig. S3 and Table S4). WT cells exhibited a biphasic APD accommodation to abrupt changes in pacing rates under drug-free conditions as observed experimentally. Notably, the simulated time constants (shown in Fig. S3 and Table S4) were close to the values experimentally recorded [17,20] and simulated in other works [19,20]. The biggest differences between WT cells and I_{Kr} mutants on APD adaptation to abrupt changes in pacing rate under drug exposure were found in $\tau_{slow\_decelarating}$ and $\tau_{slow\_accelarating}$ under Inactilide_Oi_1 exposure, specially between WT cells and activation I_{Kr} mutants (see supplemental material, Fig. S3 and Table S4).

3.6.2. Combination with other silent mutations—APD_{90} of control cells and I_{Kr} mutants under drug free conditions were prolonged in the presence of I_{Ks} or I_{NaL} silent mutations, although the extent of APD_{90} prolongation depended on the specific combination of mutations. Indeed, APD_{90} of activation, deactivation, inactivation and recovery from inactivation I_{Kr} mutants whose APD_{90} was 50 ms longer than WT under drug-free conditions exhibited a 18 ms, 24 ms, 29 ms and 29 ms prolongation in the presence of I_{Ks} silent mutations and a 18 ms, 25 ms, 25 ms and 25 ms prolongation in the presence of I_{NaL} mutations, respectively (see supplemental material, Fig. S4).

Amplification of the effects of I_{Kr} mutants on APD_{90} under drug exposure was further enhanced when I_{Kr} mutants were combined with I_{Ks} or I_{NaL} mutations, although I_{NaL} silent mutations exerted a smaller influence (Fig. S4 and Table S5). Importantly, deactivation defective mutants in combination with I_{Kr} and I_{NaL} silent mutations routinely developed EADs under exposure to low doses of Actilide_Oc and Inactilide_Oi (Fig. S4). It is to be noted that Inactilide_Oi amplified the effects of impaired inactivation and recovery from inactivation I_{Kr} in APD_{90} prolongation much more effectively in combination with latent I_{Ks}

mutants (Fig. S4). Indeed, 3.6 nM (low dose) of Inactilide_Oi_1 prolonged the effects of I_{Kr} inactivation and recovery from inactivation mutants on APD_{90} prolongation from 50 ms to 73 ms in the absence of I_{Ks} latent mutants (Fig. 4) and from 49 ms to 96 ms in the presence of I_{Ks} latent mutants (Fig. S4). The bigger influence of I_{Ks} silent mutants on the effects of defective I_{Kr} on APD_{90} than I_{NaL} silent mutants may be related to the fact that both I_{Kr} and I_{Ks} contribute to the repolarization reserve of the cells, so a reduction of both currents can create a synergistic effect on APD_{90} prolongation.

4. Discussion

4.1. Main findings

We used a computational approach to identify characteristics of drugs that selectively unmask latent, mild and moderate I_{Kr} mutations. The simulations predicted that drugs exhibiting high affinity closed-state and low affinity open-state block (Actilide_Oc) or high affinity inactivated-state and low affinity open-state block (Inactilide_Oi) unmask aLQTS arising from I_{Kr} gene variants. Exposure to such drugs caused dramatic APD prolongation in the setting of mutations causing faster I_{Kr} deactivation. By contrast, cells with impaired activation were predicted to develop the longest APDs following exposure to drugs exhibiting high affinity closed-state binding and low affinity open state block (Actilide_Oc). Addition of drugs with other properties to cells with impaired activation produced less APD prolongation. Defects in channel inactivation and recovery from inactivation were revealed with drugs exhibiting high affinity inactivated-state binding and low affinity open-state block (Inactilide Oi) while they were hidden under exposure to other types of drugs. Importantly, our method could be expanded and used to predict which type of drug would most affect any characterized I_{Kr} mutation. We have constructed a comprehensive library of mutant and drug interaction templates that can be readily modified to predict interactions of interest.

To our knowledge, this is the first time that a provocative test has been shown to selectively differentiate mutations in an ionic channel. This study, which is supported by experimental evidence, intends to be a proof of concept for future provocative tests in I_{Kr} and for the design of provocative tests in other ionic currents.

Our results suggest the specific properties of I_{Kr} blocking drugs most likely to cause aLQTS and amplify the impact of allelic variants in I_{Kr} genes in those at risk of development of drug-induced arrhythmias. This study reinforces a widely understood concept–that not all I_{Kr} block is the same. But, our results also suggest specific properties of I_{Kr} block that should be included in pre-clinical screening to ensure cardiac safety of all commercial therapeutics. Our study strongly suggests that an observation of a reduction of current comprises insufficient information to evaluate cardiac safety: screening must include kinetic measurements of hERG block.

4.2. Latent mutations

Despite the work done on the identification of proarrhythmic risk factors, prediction of the development of arrhythmic episodes in an individual subject remains unattainable [29]. It is well-known that genetic factors may increase the proarrhythmic risk, however, the

importance of altered gene expression in drug-induced TdP development is not clear [29]. Our work intends to begin to shed light on these questions and it could be used to predict the characteristics of the drugs that are more proarrhythmic in the presence of any characterized I_{Kr} mutation. In our simulations the longest drug-induced APD prolongations were observed in deactivation mutated cells (Fig. 3, second column) and most prototypical drugs preferentially prolonged APD in deactivation mutants than in WT cells, especially Actilide_Oc and Inactilide_Oi, dofetilide being notably similar to the latter. Clinical and experimental observations relating accelerated deactivation to aLQTS support our results. One patient with normal QT interval that suffered procainamide-induced arrhythmia had the M54T-hMiRP1 mutation that accelerates deactivation [1], which has been also observed in one patient among 230 patients with sporadic LQTS but not in 1010 controls [4]. Our study suggests that this latent mutation is prone to develop aLQTS especially under provocation with dofetilide-like drugs and Actilide_Oc. In addition, the S706F/KCNH2 and M756V/KCNH2 mutations have been associated to aLQTS [30]. These mutations accelerate channel deactivation and inactivation and alter the steady state inactivation curve [30]. Our study suggests that these alterations on I_{Kr} kinetics could lead to aLQTS especially in the presence of Inactilide_Oi (like dofetilide), as observed in the virtual inactivation, recovery from inactivation and deactivation mutants, and Actilide_Oc, similar to the prototypical deactivation mutants. In addition, the A561P hERG mutation, which significantly accelerates the deactivation and shifts the steady state activation curve, has been linked to LQTS and clobutinol-induced arrhythmic episodes [31]. The alterations in deactivation and activation kinetics produced by this mutation also suggest a preferential prolongation of the APD in the presence of Actilide_Oc and Inactilide_Oi.

Other I_{Kr} kinetic defects have also been implicated in aLQTS and arrhythmias, consistent with our predictions of APD prolongation resulting from altered activation, inactivation and recovery from inactivation in the presence of certain drugs (Fig. 4, first, third and fourth column). In principle, our work suggests that these mutations would be less proarrhythmic than deactivation mutants, although it also depends on the severity of the I_{Kr} alterations. The D342V/KCNH2 and H492Y/KCNH2 mutations mostly alter inactivation kinetics and have been associated with aLQTS [30]. According to our study, only analogs of drugs like Inactilide_Oi and dofetilide, would amplify the effects of these mutants. As previously mentioned, the S706F/KCNH2 and M756V/KCNH2 in addition to accelerating deactivation also accelerate inactivation [30]. Moreover, the polymorphism R104L in hERG causes defects in activation and inactivation and has been related to the incidence of TdP induced by dofetilide [32]. Indeed, our study suggests that Inactilide_Oi, like dofetilide, and Actilide_Oc could significantly prolong the APD in this mutation due to its defective inactivation and activation, respectively.

4.3. Provocative tests

Potent sodium blockers, like flecainide, have been used to unmask Brugada syndrome in patients with concealed forms of the disease [9]. More recently, a combined sodium and calcium block has been shown to be more effective for revealing this disease [10]. In addition, epinephrine and isoproterenol, which enhance beta-adrenergic stimulation, unmasked some silent LQT1 mutation carriers [8,33]. Sotalol, a potent I_{Kr} blocker, has been

shown to uncover altered repolarization [11], while another, erythromycycin, prolonged the T peak-to-end interval in LQT2 mutations, causing only modest QT prolongation in LQT1 and LQT2 mutations with normal QT interval [12]. In the aforementioned works drugs were used to reveal the genetic defects by reducing the repolarization reserve. However, in our study I_{Kr}–drug interactions are designed to reveal the specific impaired I_{Kr} kinetics. Our results indicate that unmasking of specific impaired I_{Kr} kinetics *would be possible using drugs with disparate affinities in the binding states of the I_{Kr} channel*. Our results suggest that dofetilide could be used to unmask defects in channel deactivation, inactivation and recovery from inactivation as it exhibits high affinity inactivated-state binding and low affinity open-state block (Inactilide_Oi).

When a drug exhibits variable state affinity, the extent of I_{Kr} reduction depends on the affinity of the drug in each state and the probability of residency of the channel in conformations where the drug interacts. Therefore, a mutation increasing the probability of the state where the drug is more potent will favor the block of the channel while a genetic defect decreasing that probability would minimize the block. Importantly, this mechanism could also permit the selective unmasking of silent mutations of other ionic currents, such as I_{Na} or I_{Ks}, which would improve diagnostic of all types of LQTS and, subsequently, the therapy of the LQTS.

Major advances in the pharmacological field have occurred including the automated patch-clamp, which allows high-throughput compound screening [34]. In addition, molecular modeling techniques have been implemented for the assessment of the blocking ability of drugs to the hERG1 pore domain [35]. Moreover, crystal structures of different conformational states of a K^+ channel in bacteria have been identified [36], which would allow the estimation of the differences of drug affinity in the different states of the channel. These and other new advances could be used in combination with our computational approach for drug and disease screening and identification and production of drugs or small molecules for provocative tests.

4.4. Drug safety

Our results indicate that drugs with disparate affinities to conformational states are more likely to amplify APD differences between WT and mutated cells than drugs with similar affinities to all states. Examples of drugs with disparate affinities to conformational states and related to drug-induced QT prolongation and arrhythmia are dofetilide (which exhibits a 70-fold preferential binding to the inactivated state relative to the open state), astemizole, cisapride, dl-sotalol, and terfenadine [22]. Our results also suggest that exactly these kinds of drugs should be avoided in pharmacological therapies or accompanied by I_{Kr} openers, as they could favor the appearance of aLQTS and arrhythmias in patients with common allelic variants in genes encoding the proteins constituting I_{Kr}. Therefore, the relative potency of block in the states that the drug interacts with the channels should be measured in the process of pre-clinical drug screening. Indeed, our simulations suggest that if these potencies were realized in the preclinical screen, then appropriate adjunctive therapy with a hERG channel activator could be employed to cancel any additive effects of a mutation.

Our results confirm that the risk of TdP is not solely determined by the degree of blockade of I_{Kr} [3,29]. Pharmacokinetic–pharmacodynamic relationships are known to be relevant for the development of TdP [29]. In this study, we show that the kinetics of block is crucial for amplifying the kinetic defects of the channel that prolong the APD, which may favor the generation of arrhythmias.

4.5. Limitations

In this work we used the same values of drug affinities for WT and mutated I_{Kr} cells. Severe mutations themselves can, however, modify the affinity of the drug [27] by indirect allosteric modifications in the structure of the channel protein [27]. The subtle mutations, as simulated here, would not be expected to significantly modify the structure of the channel. It is also worth mentioning that some I_{Kr} blocking drugs have been shown to modify channel trafficking [37]. In this paper, this effect has not been specifically taken into account, but would be interesting to consider with sufficient data to inform the model in future studies [37].

In this study a wide variety of virtual drugs has been simulated in order to predict the most potentially lethal combinations of drug properties and I_{Kr} kinetic abnormalities. Our results show that amplification of I_{Kr} kinetic defects on APD is observed under exposure to drugs with disparate affinities to conformational states of the I_{Kr} channel because of the differences in the residence of the channels in the binding states between the mutated and WT channels. Our study could be extended by considering an almost infinite possibility of additional virtual drugs, for example drugs with varying affinities to discrete closed states. Tools utilized in this study for simulating the effects of drugs and mutations on AP will be available upon request.

Finally, our *in silico* simulation approach allows investigations that would be difficult to undertake *in vitro*, such as precise kinetic drug properties and mutations, and the use of human cells. Our model of I_{Kr} drug interaction has been experimentally validated as it successfully reproduced drug sensitivities of two hERG mutations, N588E and N588K, to I_{Kr} dofetilide block. Although it is outside of the scope of this paper, the performance of experiments to compare drug block for WT and KCNE2 mutants at different dofetilide concentrations would be also interesting. These experiments could also be used to validate Markov simulations of channel block.

Supplementary Material

Refer to Web version on PubMed Central for supplementary material.

Acknowledgments

References

1. Sesti F, Abbott GW, Wei J, Murray KT, Saksena S, Schwartz PJ, et al. A common polymorphism associated with antibiotic-induced cardiac arrhythmia. Proc Natl Acad Sci U S A. 2000; 97:10613–8. [PubMed: 10984545]

2. Cubeddu LX, Iatrogenic QT. Abnormalities and fatal arrhythmias: mechanisms and clinical significance. Curr Cardiol Rev. 2009; 5:166–76. [PubMed: 20676275]

3. Redfern WS, Carlsson L, Davis AS, Lynch WG, MacKenzie I, Palethorpe S, et al. Relationships between preclinical cardiac electrophysiology, clinical QT interval prolongation and torsade de pointes for a broad range of drugs: evidence for a provisional safety margin in drug development. Cardiovasc Res. 2003; 58:32–45. [PubMed: 12667944]

4. Abbott GW, Sesti F, Splawski I, Buck ME, Lehmann MH, Timothy KW, et al. MiRP1 forms IKr potassium channels with HERG and is associated with cardiac arrhythmia. Cell. 1999; 97:175–87. [PubMed: 10219239]

5. Yang P, Kanki H, Drolet B, Yang T, Wei J, Viswanathan PC, et al. Allelic variants in long-QT disease genes in patients with drug-associated torsades de pointes. Circulation. 2002; 105:1943–8. [PubMed: 11997281]

6. Schwartz PJ, Priori SG, Locati EH, Napolitano C, Cantu F, Towbin JA, et al. Long QT syndrome patients with mutations of the SCN5A and HERG genes have differential responses to Na^+ channel blockade and to increases in heart rate. Implications for gene-specific therapy. Circulation. 1995; 92:3381–6. [PubMed: 8521555]

7. Rossenbacker T, Priori SG. Clinical diagnosis of long QT syndrome: back to the caliper. Eur Heart J. 2007; 28:527–8. [PubMed: 17311826]

8. Shimizu W, Noda T, Takaki H, Kurita T, Nagaya N, Satomi K, et al. Epinephrine unmasks latent mutation carriers with LQT1 form of congenital long-QT syndrome. J Am Coll Cardiol. 2003; 41:633–42. [PubMed: 12598076]

9. Brugada R, Brugada J, Antzelevitch C, Kirsch GE, Potenza D, Towbin JA, et al. Sodium channel blockers identify risk for sudden death in patients with ST-segment elevation and right bundle branch block but structurally normal hearts. Circulation. 2000; 101:510–5. [PubMed: 10662748]

10. Fish JM, Antzelevitch C. Role of sodium and calcium channel block in unmasking the Brugada syndrome. Heart Rhythm. 2004; 1:210–7. [PubMed: 15851155]

11. Kaab S, Hinterseer M, Nabauer M, Steinbeck G. Sotalol testing unmasks altered repolarization in patients with suspected acquired long-QT-syndrome–a case–control pilot study using i.v. sotalol. Eur Heart J. 2003; 24:649–57. [PubMed: 12657223]

12. Jeyaraj D, Abernethy DP, Natarajan RN, Dettmer MM, Dikshteyn M, Meredith DM, et al. I(Kr) channel blockade to unmask occult congenital long QT syndrome. Heart Rhythm. 2008; 5:2–7. [PubMed: 18273958]

13. Fink M, Noble D, Virag L, Varro A, Giles WR. Contributions of HERG K^+ current to repolarization of the human ventricular action potential. Prog Biophys Mol Biol. 2008; 96:357–76. [PubMed: 17919688]

14. O'Hara T, Virag L, Varro A, Rudy Y. Simulation of the undiseased human cardiac ventricular action potential: model formulation and experimental validation. PLoS Comput Biol. 2011; 7:e1002061. [PubMed: 21637795]

15. Perry M, Sachse FB, Sanguinetti MC. Structural basis of action for a human ether-ago-go-related gene 1 potassium channel activator. Proc Natl Acad Sci U S A. 2007; 104:13827–32. [PubMed: 17693551]

16. Pueyo E, Smetana P, Caminal P, de Luna AB, Malik M, Laguna P. Characterization of QT interval adaptation to RR interval changes and its use as a risk-stratifier of arrhythmic mortality in amiodarone-treated survivors of acute myocardial infarction. IEEE Trans Biomed Eng. 2004; 51:1511–20. [PubMed: 15376499]

17. Franz MR, Swerdlow CD, Liem LB, Schaefer J. Cycle length dependence of human action potential duration *in vivo*. Effects of single extrastimuli, sudden sustained rate acceleration and deceleration, and different steady-state frequencies. J Clin Invest. 1988; 82:972–9. [PubMed: 3417875]

18. Lau CP, Freedman AR, Fleming S, Malik M, Camm AJ, Ward DE. Hysteresis of the ventricular paced QT interval in response to abrupt changes in pacing rate. Cardiovasc Res. 1988; 22:67–72. [PubMed: 3167930]

19. Romero L, Pueyo E, Fink M, Rodriguez B. Impact of ionic current variability on human ventricular cellular electrophysiology. Am J Physiol Heart Circ Physiol. 2009; 297:H1436–45. [PubMed: 19648254]

20. Pueyo E, Husti Z, Hornyik T, Baczko I, Laguna P, Varro A, et al. Mechanisms of ventricular rate adaptation as a predictor of arrhythmic risk. Am J Physiol Heart Circ Physiol. 2010; 298:H1577–87. [PubMed: 20207815]

21. Saiz J, Gomis-Tena J, Monserrat M, Ferrero JM Jr, Cardona K, Chorro J. Effects of the antiarrhythmic drug dofetilide on transmural dispersion of repolarization in ventriculum. A computer modeling study. IEEE Trans Biomed Eng. 2011; 58:43–53. [PubMed: 20851784]

22. Perrin MJ, Kuchel PW, Campbell TJ, Vandenberg JI. Drug binding to the inactivated state is necessary but not sufficient for high-affinity binding to human ether-a-go-go-related gene channels. Mol Pharmacol. 2008; 74:1443–52. [PubMed: 18701618]

23. Demolis JL, Funck-Brentano C, Ropers J, Ghadanfar M, Nichols DJ, Jaillon P. Influence of dofetilide on QT-interval duration and dispersion at various heart rates during exercise in humans. Circulation. 1996; 94:1592–9. [PubMed: 8840849]

24. Weerapura M, Nattel S, Chartier D, Caballero R, Hebert TE. A comparison of currents carried by HERG, with and without coexpression of MiRP1, and the native rapid delayed rectifier current. Is MiRP1 the missing link? J Physiol. 2002; 540:15–27. [PubMed: 11927665]

25. Weerapura M, Hebert TE, Nattel S. Dofetilide block involves interactions with open and inactivated states of HERG channels. Pflugers Arch. 2002; 443:520–31. [PubMed: 11907818]

26. Ishii K, Nagai M, Takahashi M, Endoh M. Dissociation of E-4031 from the HERG channel caused by mutations of an amino acid results in greater block at high stimulation frequency. Cardiovasc Res. 2003; 57:651–9. [PubMed: 12618227]

27. Ficker E, Jarolimek W, Kiehn J, Baumann A, Brown AM. Molecular determinants of dofetilide block of HERG K$^+$ channels. Circ Res. 1998; 82:386–95. [PubMed: 9486667]

28. Perry M, Sachse FB, Abbruzzese J, Sanguinetti MC. PD-118057 contacts the pore helix of hERG1 channels to attenuate inactivation and enhance K$^+$ conductance. Proc Natl Acad Sci U S A. 2009; 106:20075–80. [PubMed: 19892732]

29. Hoffmann P, Warner B. Are hERG channel inhibition and QT interval prolongation all there is in drug-induced torsadogenesis? A review of emerging trends. J Pharmacol Toxicol Methods. 2006; 53:87–105. [PubMed: 16289936]

30. Itoh H, Sakaguchi T, Ding WG, Watanabe E, Watanabe I, Nishio Y, et al. Latent genetic backgrounds and molecular pathogenesis in drug-induced long-QT syndrome. Circ Arrhythm Electrophysiol. 2009; 2:511–23. [PubMed: 19843919]

31. Bellocq C, Wilders R, Schott JJ, Louerat-Oriou B, Boisseau P, Le Marec H, et al. A common antitussive drug, clobutinol, precipitates the long QT syndrome 2. Mol Pharmacol. 2004; 66:1093–102. [PubMed: 15280442]

32. Sun Z, Milos PM, Thompson JF, Lloyd DB, Mank-Seymour A, Richmond J, et al. Role of a KCNH2 polymorphism (R1047 L) in dofetilide-induced Torsades de Pointes. J Mol Cell Cardiol. 2004; 37:1031–9. [PubMed: 15522280]

33. Schechter E, Freeman CC, Lazzara R. Afterdepolarizations as a mechanism for the long QT syndrome: electrophysiologic studies of a case. J Am Coll Cardiol. 1984; 3:1556–61. [PubMed: 6715712]

34. Moller C, Witchel H. Automated electrophysiology makes the pace for cardiac ion channel safety screening. Front Pharmacol. 2011; 2:73. [PubMed: 22131974]

35. Durdagi S, Duff HJ, Noskov SY. Combined receptor and ligand-based approach to the universal pharmacophore model development for studies of drug blockade to the hERG1 pore domain. J Chem Inf Model. 2011; 51:463–74. [PubMed: 21241063]

36. Cuello LG, Jogini V, Cortes DM, Perozo E. Structural mechanism of C-type inactivation in K^+ channels. Nature. 2010; 466:203–8. [PubMed: 20613835]

37. Balijepalli SY, Anderson CL, Lin EC, January CT. Rescue of mutated cardiac ion channels in inherited arrhythmia syndromes. J Cardiovasc Pharmacol. 2010; 56:113–22. [PubMed: 20224422]

Abbreviations

aLQTS	drug-induced or acquired long-QT syndrome
AP	action potential
APD	action potential duration
APD$_{90}$	action potential duration at 90% repolarization
C1	closed state 1
C2	closed state 2
C3	closed state 3
EAD	early-afterdepolarization
ECG	electrocardiogram
I	inactivated state
I$_{Kr}$	rapid component of the delayed rectifier current
LQTS	long-QT syndrome
O	open state
RFI	recovery from inactivation
TdP	torsade de pointes
WT	wild-type
Actilide_Oc	drug binding simultaneously to both the open and closed states with lower affinity to the open state
Inactilide_Oi	drug binding simultaneously to both the open and inactivated states with lower affinity to the open state
Actilide_Co	drug binding simultaneously to both the closed and open states with lower affinity to the closed state
Inactilide_Io	drug binding simultaneously to both the inactivated and open states with lower affinity to the inactivated state
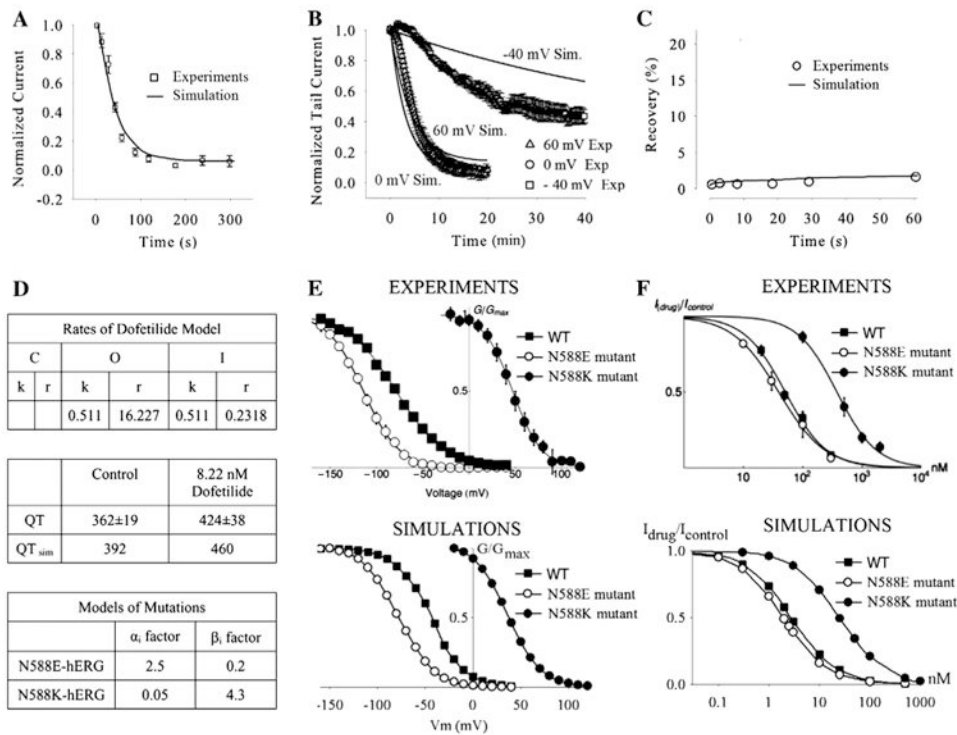
Fig. 1.

Dofetilide I_{Kr} block in WT and I_{Kr} mutant cells. Onset of WT I_{Kr} block by 50 nM dofetilide (A, B) and 3 µM dofetilide washout (C), conductance voltage curves (E) and Hill plots (F) of dofetilide-binding to WT, N588E-hERG and N588K-hERG mutants. In panels A–C, symbols correspond to experimental results [24] (A), [25] (B) and [26] (C) and solid lines represent the model predictions. Top panels and bottom panels in E and F represent the experimental [22] and the predicted results, respectively. Panel D summarizes the association (k, $µM^{-1}$ s^{-1}) and dissociation (r, 10^{-3} s^{-1}) rates for dofetilide–I_{Kr} interaction, the values of clinical [23] and simulated QT intervals at 60 bpm under drug-free and under a therapeutic dofetilide dose and the alterations introduced in the I_{Kr} model to simulate the effects of the N588E and N588K mutations. In each case, ionic concentrations and temperature (37 °C, 28 °C and 22 °C for panels A, B and C, E and F, respectively) were fixed to mimic the experimental conditions. Experimental data from [22] is reproduced with permission. Experimental data from [24] (http://onlinelibrary.wiley.com/doi/10.1113/jphysiol.2001.013296/full, DOI: 10.1113/jphysiol.2001.013296) is reproduced with permission. Experimental data from [25] is reproduced with kind permission from Springer Science and Business Media. The onset of block by 0.5 µM dofetilide with repetitive pulsing is voltage-dependent. Two-second depolarizing pulses to –40, 0 or +60 mV were applied with a 12-s interpulse interval (IPI). Pulses to –40 mV were applied for a longer period to allow for steady-state inhibition. All values are mean ± SEM (n=4, 3 and 4 for –40, 0 and +60 mV respectively). Experimental data from [26] is reproduced by permission of Oxford University Press.
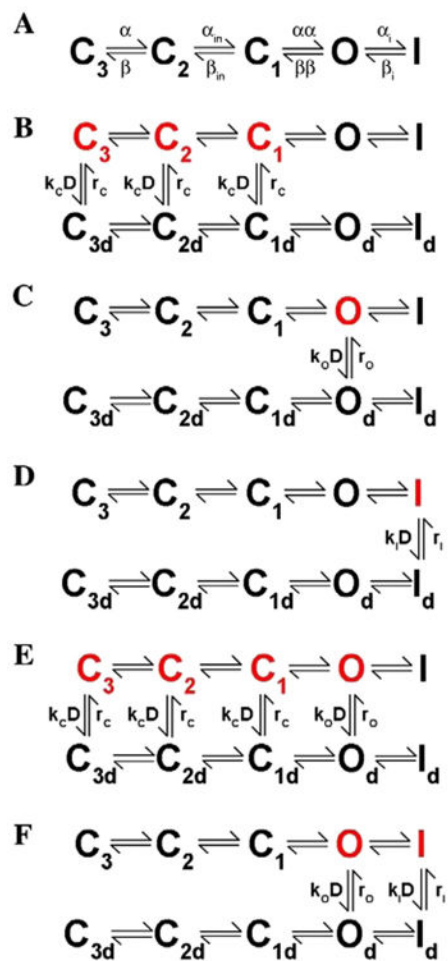
Fig. 2.
Fink et al. Markov model of the human I_{Kr} channels [13] (A) and simulated drug–I_{Kr} interaction models (B, C, D, E, F) with nondrug bound and drug bound estates (d), k_C, k_O and k_I are the association rates constants in the closed, open and inactivated states, respectively, D is the drug concentration and r_C, r_O and r_I are the dissociation rate constants in the closed, open and inactivated states, respectively. Binding states are red colored.
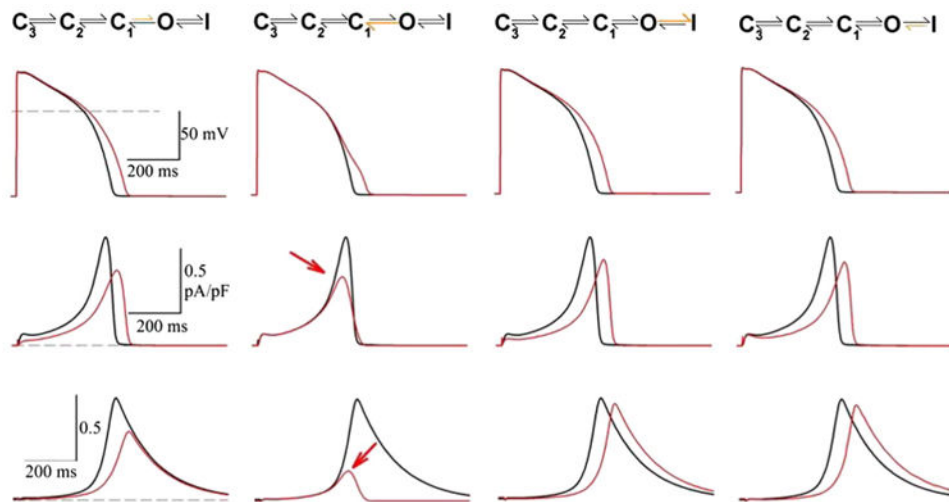
Fig. 3.
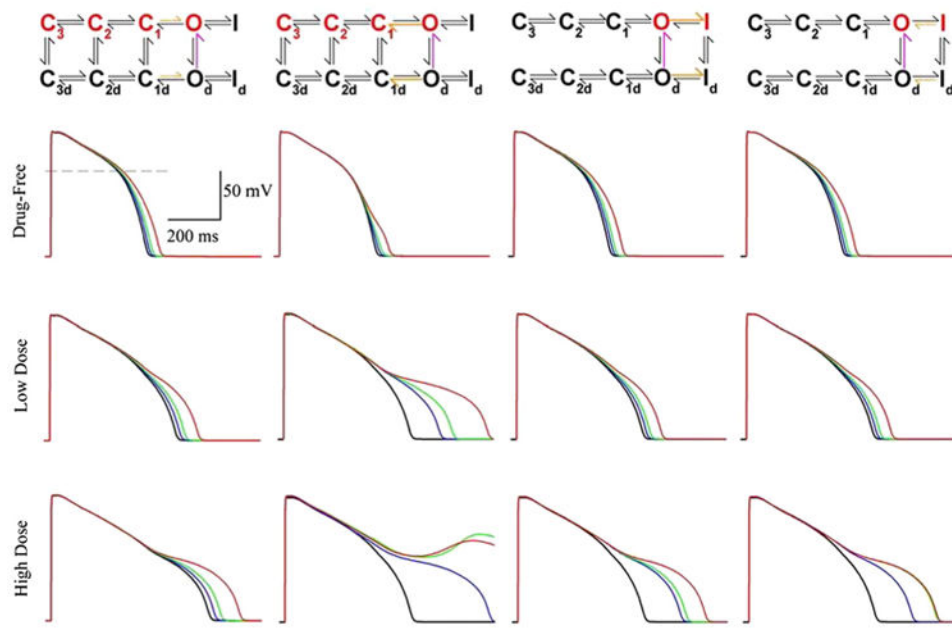Simulated steady state AP (top row), I_{Kr} (middle row) and open state probability (bottom row) for endocardial WT (black) and mutated cells with altered I_{Kr} activation (first column), deactivation (second column), inactivation (third column) and recovery from inactivation (forth column) producing a 50 ms (red) APD_{90} prolongation under drug-free conditions. Markovian schemes of the simulated I_{Kr} mutants are depicted at the top. The orange arrows represent the transition rate that has been altered to simulate each mutation.

Fig. 4.
Simulated steady state AP for endocardial WT (black) and mutated cells with altered I_{Kr} activation (first column), inactivation (second column), deactivation (third column) or recovery from inactivation (fourth column) producing a 10 ms (blue), 20 ms (green) and 50 ms (red) APD$_{90}$ prolongation under drug-free conditions (top row) and in the presence of low (middle row) and high (bottom row) doses of Actilide_Oc_1 (first and second column) or Inactilide_Oi_1 (third and fourth column) (supplemental material, Table S3). Markovian schemes of the simulated drug–channel interactions are depicted at the top. The orange arrows represent the transition rate that has been altered to simulate each mutation and the pink arrow indicates that the drug has a low affinity in that binding state.
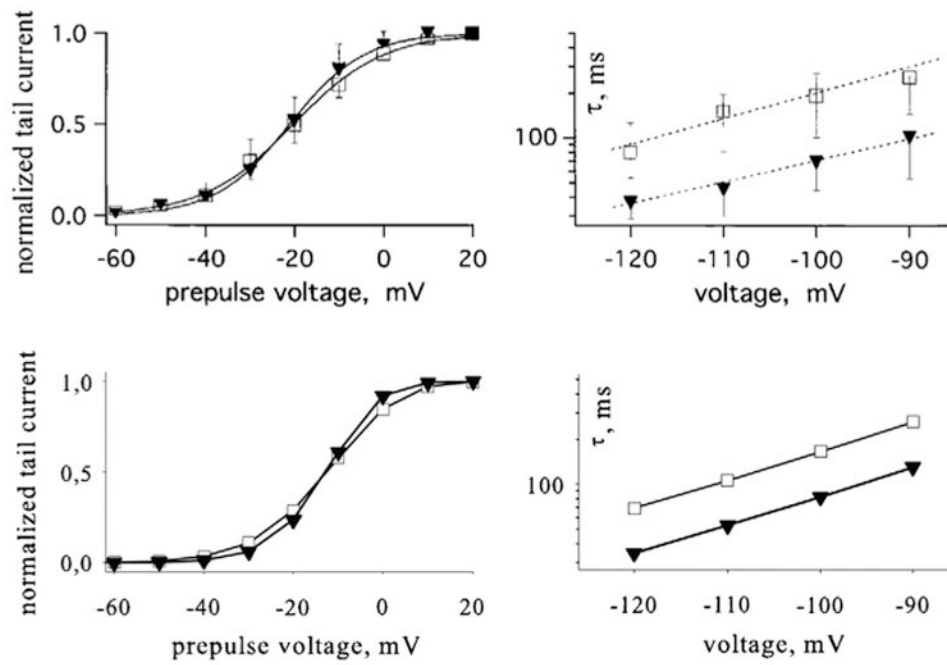
Fig. 5.
Experimental (top panels) [4] and simulated (bottom panels) steady-state activation (A and C) and deactivation time constants for WT (squares) and M54T hMiRP1 mutated (triangles) channels at 22 °C. Top panels are reprinted from [4] with permission from Elsevier.
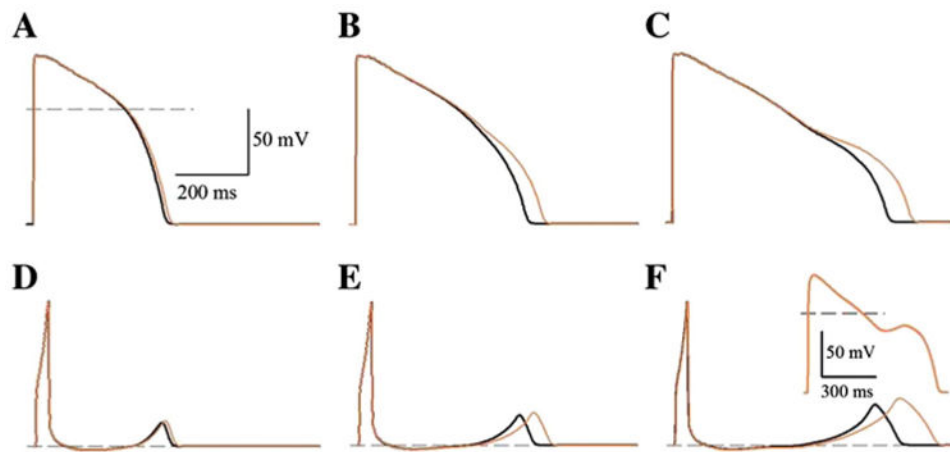
Fig. 6.
Simulated steady state AP of isolated endocardial cells (top row) and pseudo-ECG (bottom row) for WT (black) and M54T hMiRP1 cells (orange) in the absence (left column) and in the presence of 16 nM (low dose) and 48 nM (high dose) of dofetilide (middle and right column, respectively). Inset of panel F shows the AP of midmyocardial cell#85 of the 1D model of the mutated transmural wedge preparation.
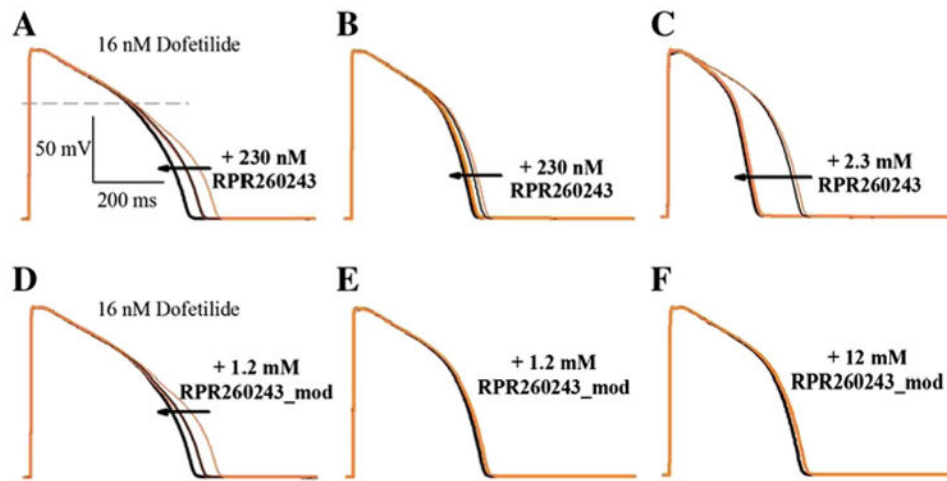
Fig. 7.
Simulated steady state AP for endocardial WT (black) and M54T hMiRP1 cells (orange) in the absence (thin) and in the presence (thick) of real (top row) and prototypical (bottom row) I_{Kr} activators under different conditions: in the presence of low dose (16 nM) dofetilide (first column) and under I_{Kr} blocker drug free conditions (middle and last column). I_{Kr} activator dose is indicated in each panel.
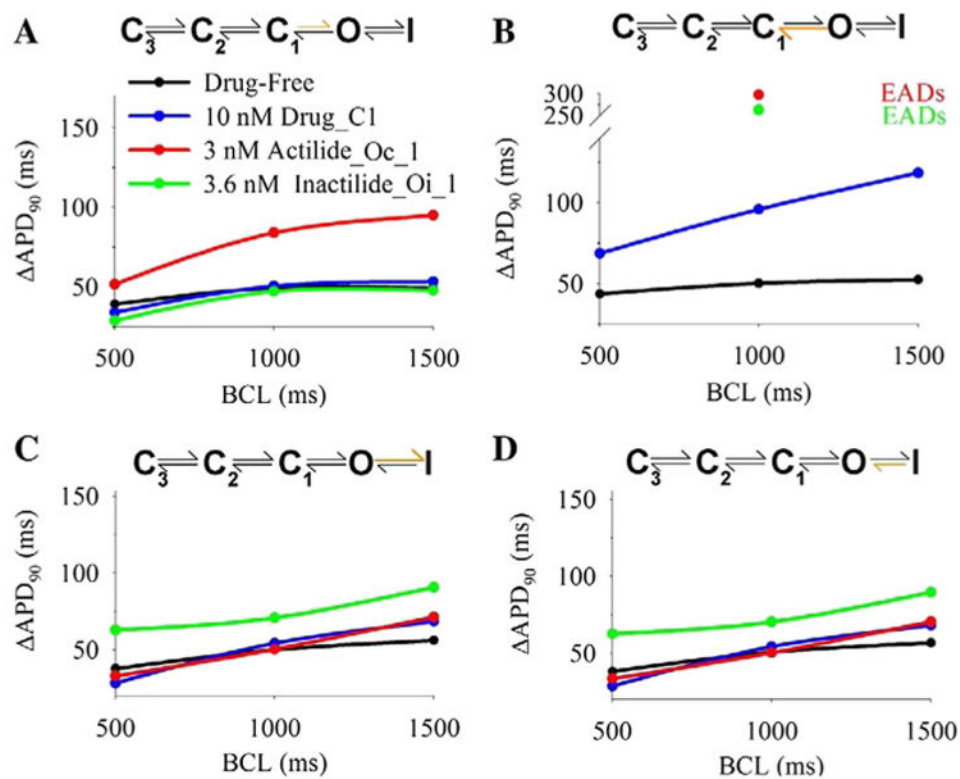
Fig. 8.
Rate dependence of the effects of I_{Kr} mutants on ADP_{90} under drug-free conditions (black) and under exposure to low doses of those drugs that significantly amplify them, namely Actilide Oc_1 (red), Inactilide_Oi_1 (green) and Drug_C1 (blue) (supplemental material, Table S3). ADP_{90} differences between WT cells and mutated cells with altered I_{Kr} activation (A), deactivation (B), inactivation (C) and recovery from inactivation (D) producing a 50 ms (red) APD_{90} prolongation under drug-free conditions at 1 Hz. ADP_{90} differences between WT cells and mutated cells with altered I_{Kr} deactivation under exposure to low doses of Actilide Oc_1 (red) and Inactilide_Oi_1 (green) at 2 Hz is not shown as mutated cells were stimulated before the repolarization process was completed. Markovian schemes of the simulated I_{Kr} mutants are depicted at the top. The orange arrows represent the transition rate that has been altered to simulate each mutation.